Journal of Biomolecular Structure and Dynamics
Publication details, including instructions for authors and subscription information:
http://www.tandfonline.com/loi/tbsd20

Carbon monoxide binding to the heme group at the dimeric interface modulates structure and copper accessibility in the Cu,Zn superoxide dismutase from Haemophilus ducreyi: in silico and in vitro evidences

Giovanni Chillemi [a], Serena De Santis [b], Mattia Falconi [c], Giordano Mancini [a], Valentina Migliorati [b], Andrea Battistoni [c], Francesca Pacello [c], Alessandro Desideri [c] & Paola D'Angelo [b]

[a] CASPUR, Consortium for Supercomputing Applications, Rome, Italy
[b] Department of Chemistry, University of Rome "La Sapienza", Rome, Italy
[c] Department of Biology, University of Rome Tor Vergata, Rome, Italy

Available online: 11 Jun 2012

To cite this article: Giovanni Chillemi, Serena De Santis, Mattia Falconi, Giordano Mancini, Valentina Migliorati, Andrea Battistoni, Francesca Pacello, Alessandro Desideri & Paola D'Angelo (2012): Carbon monoxide binding to the heme group at the dimeric interface modulates structure and copper accessibility in the Cu,Zn superoxide dismutase from Haemophilus ducreyi: in silico and in vitro evidences, Journal of Biomolecular Structure and Dynamics, DOI:10.1080/07391102.2012.680028

To link to this article: http://dx.doi.org/10.1080/07391102.2012.680028

Journal of Biomolecular Structure and Dynamics
iFirst, 2012, 1–11

Carbon monoxide binding to the heme group at the dimeric interface modulates structure and copper accessibility in the Cu,Zn superoxide dismutase from *Haemophilus ducreyi*: in silico and *in vitro* evidences

Giovanni Chillemi[a]*, Serena De Santis[b], Mattia Falconi[c], Giordano Mancini[a], Valentina Migliorati[b], Andrea Battistoni[c], Francesca Pacello[c], Alessandro Desideri[c] and Paola D'Angelo[b]

[a]*CASPUR, Consortium for Supercomputing Applications, Rome, Italy;* [b]*Department of Chemistry, University of Rome "La Sapienza", Rome, Italy;* [c]*Department of Biology, University of Rome Tor Vergata, Rome, Italy*

Communicated by Ramaswamy H. Sarma

(*Received 21 December 2011; final version received 23 February 2012*)

X-ray absorption near-edge structure (XANES) spectroscopy and molecular dynamics (MD) simulations have been jointly applied to the study of the Cu,Zn superoxide dismutase from *Haemophilus ducreyi* (HdSOD) in interaction with the carbon monoxide molecule. The configurational flexibility of the Fe(II)-heme group, intercalated between the two subunits, has been sampled by MD simulations and included in the XANES data analysis without optimization in the structural parameter space. Our results provide an interpretation of the observed discrepancy in the Fe-heme distances as detected by extended X-ray absorption fine structure (EXAFS) spectroscopy and the classical XANES analysis, in which the structural parameters are optimized in a unique structure. Moreover, binding of the CO molecule to the heme induces a long range effect on the Cu,Zn active site, as evidenced by both MD simulations and *in vitro* experiments. MD simulation of the CO bound system, in fact, highlighted a structural rearrangement of the protein–protein hydrogen bond network in the region of the Cu,Zn active site, correlated with an increase in water accessibility at short distance from the copper atom. In line, *in vitro* experiments evidenced an increase of copper accessibility to a chelating agent when the CO molecule binds to the heme group, as compared to a heme deprived HdSOD. Altogether, our results support the hypothesis that the HdSOD is a heme-sensor protein, in which binding to small gaseous molecules modulates the enzyme superoxide activity as an adaptive response to the bacterial environment.

Keywords: Cu,Zn superoxide dismutase; heme-sensor proteins; X-ray absorption spectroscopy; XANES; molecular dynamics simulation; heme group; metalloproteins

Introduction

Haemophilus ducreyi, the causative agent of the sexually transmitted human genital ulcerative disease known as chancroid, expresses one of the most interesting examples of bacterial Cu,Zn superoxide dismutases (HdSOD). Its N-terminal domain, in fact, is characterized by a histidine-rich region followed by a methione-rich sequence, capable of binding both Copper(I) and Copper(II) (D'Angelo et al., 2005; Pacello et al., 2001). However, the most striking feature of this metalloenzyme is the ability to bind a heme molecule at the interface between the two subunits (see Figure 1) (Pacello et al., 2001; Törő et al., 2009). It is noteworthy that this feature of HdSOD seems to be related to the fact that *H. ducreyi* is unable to synthesize heme but acquires this cofactor from humans, its only known host, and can use it as a suitable iron source. The role of heme in HdSOD is still debated and it has been hypothesized that the enzyme could play a role in protection from heme toxicity (Negari et al., 2008). Another possibility is that heme could serve as a cofactor for additional catalytic activities useful to protect the micro-organism from reactive nitrogen or oxygen intermediates produced during the phagocytic oxidative burst. In this respect, it has been shown that HdSOD is able to bind small gaseous ligands, such as nitric oxide or carbon monoxide, as a sixth ligand of heme thus displacing the distal histidine (D'Angelo et al., 2010; Vos et al., 2008). These last experimental observations allow one to speculate on a possible role of HdSOD as a heme-based-sensor protein, regulating the adaptive responses to fluctuating oxygen, carbon monoxide, or nitric oxide levels (Gilles-Gonzalez & Gonzalez, 2005).

*Corresponding author. Email: g.chillemi@caspur.it

ISSN 0739-1102 print/ISSN 1538-0254 online

http://dx.doi.org/10.1080/07391102.2012.680028
http://www.tandfonline.com

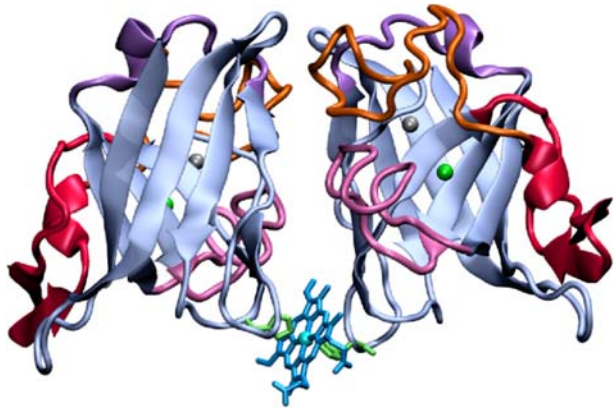

Figure 1. 3D structure of HdSOD. The Cu,Zn active sites are buried in the structured β-barrel regions. Conserved regions among prokaryotes and eukaryotic organisms are highlighted in different colors: SS subloop (residues Glu73-Gly93) in red color; Zn subloop (residues Gly94-Ala119) in orange color; Greek key loop (residues Pro135-Gly145) in violet color; and 7,8 loop (residues Ala152-Pro169) in pink color.

Recently, ferric, ferrous, CO-, and NO-bound HdSOD in solution have been investigated by X-ray absorption spectroscopy (XAS) to measure the structural modifications induced by the binding of small gaseous ligands to heme in this enzyme. The combined analysis of extended X-ray absorption fine structure (EXAFS) and X-ray absorption near edge structure (XANES) data has allowed the characterization of the local structure around the Fe-heme with .02 Å accuracy, revealing an elongation in the axial site of the Fe-proximal histidine distance upon coordination of the CO/NO molecule (D'Angelo et al., 2010). A discrepancy between the EXAFS and XANES determinations, however, was observed in the Fe-proximal histidine distance in the CO/NO bound systems and in the Fe-distal histidine distance of the HdSOD system. An analogous systematic error between EXAFS and XANES has been recently observed in neuroglobin and it was demonstrated to be due to the configurational disorder associated with the distortion of the heme plane and with the different orientations of the axial ligands, which are not taken into account in the standard XANES analysis (from now on referred as "static XANES" analysis) (D'Angelo et al., 2010). The discrepancy, in fact, disappears applying a novel strategy that combines XANES and molecular dynamics (MD), from now on referred as "dynamic XANES" analysis.

In order to investigate the structural and dynamic response of HdSOD to the binding of CO to heme, we carried out MD simulations of the enzyme in the absence (HdSOD) or the presence of the sixth CO ligand (CO-HdSOD). The conformational sampling allowed us to apply the "dynamic XANES" analysis to prove that it solves the observed discrepancy between EXAFS and "static XANES." Moreover, the two 100 ns long MD simulations highlighted structural modifications in the HdSOD Cu,Zn active site upon binding of the CO molecule that are correlated with a greater accessibility of the copper ion. In line, an ad hoc experiment confirmed a greater accessibility of the copper ion in CO-HdSOD as compared with HdSOD devoid of the heme group.

Materials and methods

X-ray absorption measurements

Fe K-edge X-ray absorption spectra of HdSOD were collected in fluorescence mode at the BM30B FAME beamline of the European Synchrotron Radiation Facility (ESRF). To a 1.47 mM solution of heme-bound HdSOD in the Fe(III) oxidation state dissolved in 35 mM HEPES pH 7.4 and 30% glycerol, a 10 mM solution of sodium dithionite was added under nitrogen atmosphere to collect the chemically reduced species. The CO-derivative (CO-HdSOD) was obtained by reducing the ferric sample with 10 mM sodium dithionite in carbon monoxide atmosphere. All the spectra were collected at 5 K to prevent the sample from X-ray damages. The storage ring was running in the two-thirds filling mode with a typical current of 170 mA. The monochromator was equipped with a Si(2 0 0) double crystal, in which the second crystal was elastically bent to a cylindrical cross section. The X-ray photon beam was vertically focused by a Rh mirror and dynamically sagittally focused in the horizontal size. An array detector made of 30 Ge elements of very high purity was used. The spectra were calibrated by assigning the first inflection point of the Fe foil spectrum to 7111.2 eV. For the HdSOD system, XAS spectra were recorded with a 7 s/point collection statistic and averaged. No spectral changes were detected during the data collection. For the CO-HdSOD system, a clear spectral evolution was observed when the beam spot was kept fixed. Therefore, it was necessary to move the beam spot to different positions on the sample, and three equal spectra were collected and averaged for the XAS analyses of the CO derivative.

XANES data analysis

The XANES data analysis was carried out with the MXAN code (Benfatto & Della Longa, 2001). The X-ray photoabsorption cross section is calculated using the full multiple scattering scheme in the framework of the muffin-tin approximation for the shape of the potential. All details on the potential calculations can be found in D'Angelo et al. (2010). The exchange and correlation parts of the potential are determined on the basis of the local density approximation of the self-energy. The real part of self-energy is calculated by using the Hedin–

Lundqvist (HL) energy-dependent potential. In the first step, the XANES spectrum associated with each MD configuration was calculated using only the real part of the HL potential; i.e. theoretical spectra do not account for any intrinsic and extrinsic inelastic process, while the damping associated with the experimental resolution is accounted for by convolution with a Gaussian function with full width at half-maximum (fwhm) of .7 eV. In the second step, to perform a comparison with the experimental data, the damping associated with the inelastic processes has to be included in the calculation. To this purpose, we used a modified version of the MXAN program that reads an external theoretical spectrum (the configurational averaged calculated data) and performs a minimization in the nonstructural parameter space only. In particular, the inelastic processes are accounted for by convolution with a broadening Lorentzian function having an energy-dependent width of the form $\Gamma(E) = \Gamma_c + \Gamma_{mfp}(E)$. The constant part Γ_c accounts for the core-hole lifetime and is fixed to the tabulated value of 1.55 eV fwhm, while the energy-dependent term represents all the intrinsic and extrinsic inelastic processes (D'Angelo et al., 2010). The $\Gamma_{mfp}(E)$ function is zero below an energy onset E_s (which in extended systems corresponds to the plasmon excitation energy) and starts increasing from a given value A, following the universal functional form of the mean free path in solids (Muller, Jepsen, & Wilkins, 1982). Both the onset energy E_s and the jump A are introduced in the $\Gamma_{mfp}(E)$ function via an arctangent functional form to avoid discontinuities. Least-squares fits of the XANES experimental data have been performed by minimizing the χ^2 function, defined as

$$\chi^2 = \frac{1}{m\varepsilon^2}\sum_{i=1}^{m}[(y_i^{th} - y_i^{exp})\varepsilon_i^{-1}]^2 \qquad (1)$$

where m is the number of experimental points, y_i^{th} and y_i^{exp} are the theoretical and experimental values of the absorption cross section, and ε_i is constant and equal to .5% of the experimental jump.

An important question when dealing with the computation of spectra from MD simulations is to determine the total sampling length that is necessary to have a statistically significant average. To this end, we carried out a statistical analysis of the errors associated with the averaged theoretical spectra. In particular, an averaged XANES spectrum over N configurations is affected by a variance $\sigma^2(E_i)/N$, so for any N it is possible to calculate an energy-dependent error bar defined as $\pm\sigma(E_i)/N^{1/2}$.

Force field and MD simulations

We carried out two MD simulations, each 100 ns long, of the HdSOD and CO-HdSOD systems in which the EXAFS distances were assigned to the equilibrium geometry of the heme group (see Table 1). The starting coordinates for the HdSOD system were taken from the X-ray structure of HdSOD at 1.5 Å resolution (PDB code 1Z9 N). The approximated CO and distal histidine positions in the CO bound structure were obtained by combining the X-ray structure of HdSOD and the CO-bound ferrous murine neuroglobin at 1.7 Å resolution (PDB code 1W92) (Vallone, Nienhaus, Matthes, Brunori, & Nienhaus, 2004). In order to determine the partial charges of the hexacoordinated heme in HdSOD and CO-HdSOD, B3LYP calculations were carried out on the isolated bis(imidazole) iron(II) porphyrin [Fe(II)P$(Im)_2$] complex and the carboxy-imidazole iron(II) porphyrin [Fe(II)P(CO)(Im)] complex (Becke, 1993). We used the Dunning's triple zeta basis set (Schaefer, Horn, & Ahlrichs, 1992) for the iron; the 6-311+G* basis set for the nitrogen atoms of the heme and the heteroatoms of the imidazole and carbon monoxide molecules; and the 3-21G basis set for the rest of the system and for all hydrogen atoms. In the calculations, both the [Fe(II)P$(Im)_2$] and [Fe(II)P(CO)(Im)] complexes were assumed to be in the singlet, closed-shell state following previous studies (D'Angelo et al., 2010; Harvey, 2000; Li, Ai, Xie, & Fang, 2008; Loew & Harris, 2000; McMahon, Stojkovic, Hay, Martin, & Garcia, 2000; Smith, Dupuis, & Straatsma, 2005).

Table 1. Fe(II)-heme geometrical parameters for HdSOD and CO-HdSOD obtained by XANES (static analysis) and EXAFS, from D'Angelo et al., (2010).

	XANES (static analysis)	EXAFS
HdSOD		
Fe–N_{pyrrol} (Å)	2.00(2)	1.98(2)
Fe–N_{His} proximal (Å)	1.90(4)	1.97(3)
Fe–N_{His} distal (Å)	2.02(7)	2.03(4)
CO-HdSOD		
Fe–N_{pyrrol} (Å)	2.01(2)	1.99(2)
Fe–N_{His} proximal (Å)	1.93(7)	2.08(4)
Fe–CO (Å)	1.86(5)	1.82(3)
Fe–C–O (°)	179(12)	179(10)
CO (Å)	1.10[a]	1.10(2)

[a]fixed

All our quantum chemical calculations were carried out using the Gaussian03 (verD02) package Frisch et al., 2009. The partial charges were obtained from the CHELPG algorithm (Breneman & Wiberg, 1990) and the fitted charges were constrained to exactly reproduce the total charge and the calculated dipole moment of the system. The obtained set of partial charges are: .86 e (electronic charge) for the iron, −.33 e for the pyrrolic nitrogen atoms in the HdSOD system; .56 e for the iron, −.23 e for the pyrrolic nitrogen atoms, .23 e for the carbon and −.24 e for the oxygen atom in the CO-HdSOD system.

Partial electrostatic charges for the active Cu,Zn active sites, composed also by residues His70, His72,

His95, His104, His113, His151, and Asp116, were obtained from Shen and coauthors (Shen, Wong, Subramaniam, Albright, & McCammon, 1990). The two protein structures have been immersed in cubic water boxes with explicit single point charge water molecules (Berendsen, Postma, van Gunsteren, & Hermans, 1981) imposing a minimal distance between the solute and the box walls of 13 Å. The systems were neutralized with 2 Na^+ counterions placed in electrostatically preferred positions. The total number of atoms is nearly 95,000 for the two systems. MD simulations were performed with the Gromacs software package (Berendsen, van der Spoel, & van Drunen, 1995) using the GROMOS96 force field (Van Gunsteren et al., 1996). The additional parameters for hexacoordinated heme and bound CO were taken from the GROMOS force field parameter sets 53A6 (Oostenbrink, Villa, Mark, & van Gunsteren, 2004), with the exception of Fe–N_{pyrrol}, Fe–$N_{His,}$ and Fe–CO equilibrium atomic distances that have been fixed to the EXAFS results (see Table 1) (D'Angelo et al., 2010). A second force field of CO-HdSOD has also been generated with the "static XANES" geometry, in order to verify the sensitivity of the "dynamic XANES" analysis on structural changes around the scattering atom.

The initial velocities were taken randomly from a Maxwellian distribution at 300 K, and the temperature was held constant by the V-rescale algorithm (Bussi, Donadio, & Parrinello, 2007). The Particle Mesh Ewald method (Essmann et al., 1995) was used for calculation of the long range interactions. For all systems, the solvent was relaxed by energy minimization followed by 100 ps of MD at 300 K while restraining protein atomic positions with a harmonic potential. The systems were then minimized without restraints, and their temperature was brought to 300 K in a stepwise manner: 500 ps MD runs were carried out at 50, 100, 150, 200, 250, and 300 K, before starting the production runs at 300 K.

Both the HdSOD and CO-HdSOD systems, in which the EXAFS distances were assigned to the equilibrium geometry of the heme group, were simulated for 100 ns. The CO-HdSOD system, in which the "static XANES" distances were assigned to the equilibrium geometry of the heme group, was simulated for 10 ns starting from the last configuration of the 100 ns long previously described simulation of CO-HdSOD.

All the simulation analyses were carried out over the equilibrated MD trajectories using the standard tools present in GROMACS MD package version 4.0.7 (Hess, Kutzner, van der Spoel, & Lindahl, 2008). The per-residue root mean square fluctuations (RMSF) have been calculated by removing the global translations and rotations.

The structural properties of the water molecules interacting with the Cu(II) ions have been described in terms of radial distribution functions, $g_{AB}(r)$:

$$g_{AB}(r) = \frac{(\rho_B(r))}{(\rho_B)_{local}} = \frac{1}{N_A(\rho_B)_{local}} \quad (2)$$

where $(\rho_B(r))$ is the particle density of type B at distance r around type A and $(\rho_B)_{local}$ is the particle density of type B averaged over all spheres around particle A with radius r_{max} (half the box length).

Copper release from the active site

Recombinant heme-containing and heme-devoid mutant HdSOD, lacking the first 22 residues, were purified as previously described (Battistoni et al., 2001; Pacello et al., 2001); HdSOD samples at a concentration of .01 mg/ml were incubated at room temperature in 50 mM Hepes buffer pH 7.3, 6 mM sodium dithionite as reducing agent and 0.1 mM BCS (bathocuproinedisulfonic acid) as chelating agent. The CO-derivatives of the two systems were obtained in carbon monoxide atmosphere in sealed tubes. After an incubation of 24 h, aliquots were withdrawn and immediately assayed for residual activity by the pyrogallol method (Marklund & Marklund, 1974). The percent residual activity values were obtained from the ratio between the activity of CO/BCS/$Na_2S_2O_4$ heme devoid-HdSOD or CO/BCS/$Na_2S_2O_4$ heme-HdSOD and that of an equal amount of $Na_2S_2O_4$ heme devoid-HdSOD and $Na_2S_2O_4$ heme-HdSOD, respectively. Each value is the mean of three independent measurements. The statistical analysis of results was carried out with Sigma Stat.

Results and discussion

Dynamic XANES analysis

The "dynamic XANES" analysis of the heme Fe(II) HdSOD and CO-HdSOD systems, i.e. a quantitative analysis of the XANES spectra using the conformational space visited by the 100 ns long MD simulations, has been carried out to take into account the structural disorder effects on the low-energy portion of the XAS spectra. The results for HdSOD are reported in Figure 2. Panel A shows 300 XANES theoretical spectra associated to different instantaneous configurations extracted from the MD simulation (black lines), together with the XANES average theoretical spectrum (red line). The calculated XANES spectra present a noticeable fluctuation up to 100 eV after the edge, demonstrating the sensitivity of XANES to the geometrical changes visited by the MD simulation, while the EXAFS region above this value is less sensitive to the configurational variations. For each energy point of the average theoretical spectrum calculated from 300 MD frames, we have calculated the error bars reported in red in panel B (see Materials and Methods). The small entity of the errors

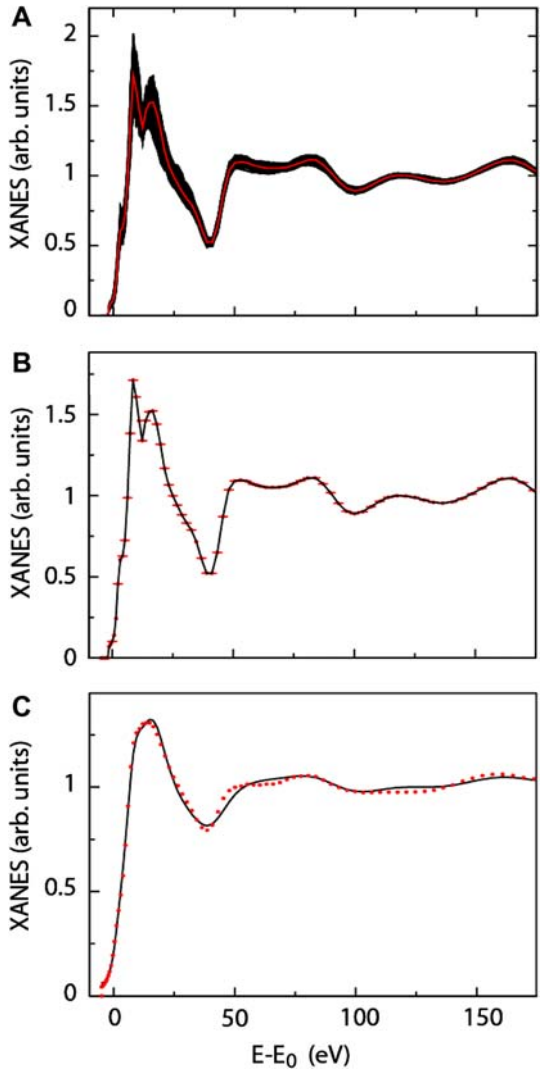

Figure 2. (A) Comparison of the theoretical XANES spectrum of HdSOD obtained from the MD average (red line) and several spectra associated with individual MD configurations (black lines); (B) MD average theoretical XANES spectrum of HdSOD (black line) with statistical error bars (red lines); and (C) comparison between the MD average theoretical XANES spectrum of HdSOD (black line) and the experimental data (red dotted line).

demonstrates that 300 frames are sufficient to reach a statistically significant convergence.

To assess the reliability of the theoretical results, the XANES average theoretical spectrum has been compared with the experimental data. To this end, all inelastic processes have been accounted for by convoluting the theoretical averaged spectra with a broadening Lorentzian function and the corresponding nonstructural parameters (E_s and A) have been optimized together with the E_0 value, for a total of only three fitted parameters. Figure 2 panel C shows that the agreement between the experimental and theoretical curves is good ($\chi^2 = 1.12$), better than the one obtained from the "static" analysis ($\chi^2 = 1.74$), despite the smaller number of optimized parameters. In the "static XANES" analysis, in fact, minimization of the χ^2 function was performed in the space of eight parameters: three structural parameters (the heme-core size, leading to the Fe–N_{pyrrol} distance, and the two Fe–N_{His} distances associated with the proximal and distal histidines) and five nonstructural parameters, Γ_c (the core-hole width), E_s^{normal}, E_s^{heme}, A_s^{normal}, and A_s^{heme} (associated with the phenomenological broadening function).

These results demonstrate that the systematic error in the determination of the Fe-distal histidine distance, arising from the use of a single configuration, is eliminated by the "dynamic XANES" analysis procedure, as already observed in the case of neuroglobin, and the Fe-heme distances obtained by the EXAFS analysis are confirmed.

In the case of CO-HdSOD, due to both the high flexibility of the heme pocket and the high disorder associated with the different orientations of the histidine and CO molecule, the configurational disorder on the XANES spectrum is larger than in HdSOD. This increases the discrepancy between EXAFS and "static XANES" determinations (see Table 1). Also, in this case the "dynamic XANES" analysis, carried out on selected configurations obtained by the MD simulation using the EXAFS distances, produces a theoretical XANES spectrum at convergence in 300 frames (see Figure 3, panel A) and in a very good agreement with the experimental one (see Figure 3, panel B). The χ^2 values obtained in the "static" and "dynamic XANES" analyses, in fact, are 1.58 and 1.20, respectively.

To gain a deeper insight into the sensitivity of the "dynamic XANES" procedure towards structural changes of the sampled heme-ligand geometry, we carried out an additional MD simulation of CO-HdSOD using the Fe-heme geometry obtained from the "static XANES" analysis (see Table 1 and Materials and Methods). In particular, the main difference between the Fe-heme force field previously described and this one is the shortening of the Fe–N_{his} proximal distance from 2.08 Å (EXAFS determination) to 1.93 Å ("static XANES" determination). The results, reported in Figure 3 panels C and D, show that the theoretical spectrum is different from that obtained in the simulation using the EXAFS distances for the Fe-heme geometry (compare Figure 3 panel A vs. C), demonstrating that the "dynamic XANES" procedure is sensitive to small differences in the scattering center structure. The comparison between the experimental XANES data of CO-HdSOD and the theoretical MD average spectra calculated using the XANES static distances is shown in Figure 3 panel D. A quite good agreement is obtained also in this case ($\chi^2 = 1.20$), but a better reproduction of the experimental XANES features

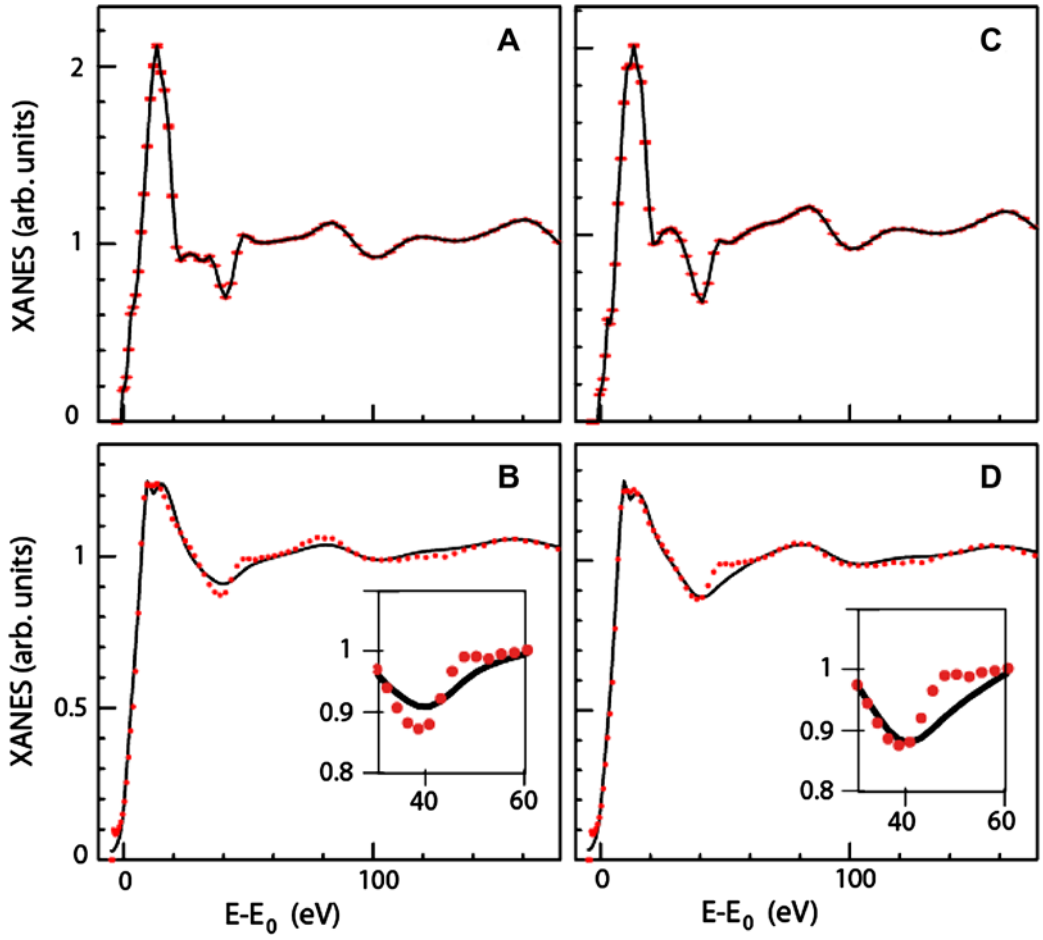

Figure 3. (A) MD average theoretical XANES spectrum of CO-HdSOD using the Fe-heme geometry obtained from the EXAFS analysis (black line) with statistical error bars (red lines); (B) MD average theoretical XANES spectrum of CO-HdSOD using the Fe-heme geometry obtained from the "static XANES" analysis (black line) with statistical error bars (red lines); (C) comparison between the MD average theoretical XANES spectrum of CO-HdSOD using the Fe-heme geometry obtained from the EXAFS analysis (black line) and the experimental data (red dotted line); and (D) comparison between the MD average theoretical XANES spectrum of CO-HdSOD using the Fe-heme geometry obtained from the "static XANES" analysis (black line) and the experimental data (red dotted line).

in the energy region between 20 and 40 eV is obtained in the case of the MD simulation using EXAFS distances (compare inserts in panel B vs. D). Note that this XAS region is known to be a fingerprint of the heme axial coordination (D'Angelo et al., 2008).

The very good reproduction of XANES experimental data for HdSOD and CO-HdSOD, when using the force field with the Fe-heme geometry determined by the EXAFS analysis, makes us confident on the whole conformational sampling obtained by the two 100 ns long MD simulations, that, therefore, have been analyzed to gain a deeper insight into the structural and dynamic characteristics of this enzyme.

Root mean square deviations and fluctuations

The root mean square deviations (RMSD) measure the deviation of the simulated structures from the X-ray starting structure. The backbone HdSOD and CO-HdSOD RMSD shows a steep increase during the first 5 ns (see Figure 4, panel A) reaching a value around 2.5 and 2.0 Å, respectively, while in the remaining part of the simulation time the values oscillate around 3.0 Å. Elimination of the loops (see Figure 1 for their definition) reduces the RMSD of both systems, since a large portion of flexibility is located in these regions, in line with what observed in other bacterial SODs (De Maria et al., 2002; Falconi et al., 2001). However, it is interesting to note that the total backbone RMSD in CO-HdSOD is slightly lower than in HdSOD, while upon removing of the loops from the analysis, the backbone RMSD is lower in the HdSOD system than in the CO-HdSOD one (see Figure 4, panel B). Therefore, binding of the CO molecule reduces the deviations of the loops from the starting structure, while it increases the ones of

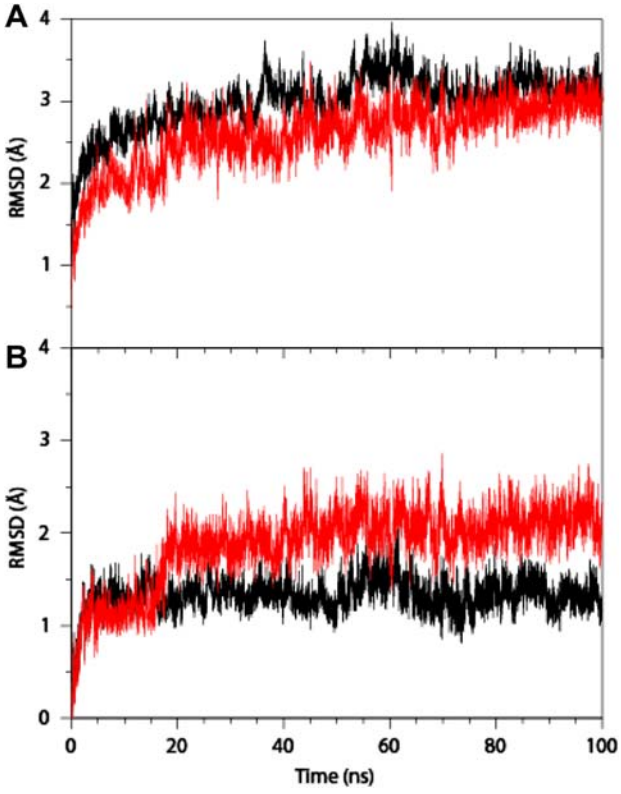

Figure 4. RMSD HdSOD and CO-HdSOD from X-ray starting structure are reported in black and red lines, respectively. Panel A backbone deviations; Panel B same as Panel A with the elimination of the loop residues from the analysis, i.e. SS subloop (residues Glu73-Gly93); Zn subloop (residues Gly94-Ala119); Greek key loop (residues Pro135-Gly145); and 7,8 loop (residues Ala152-Pro169).

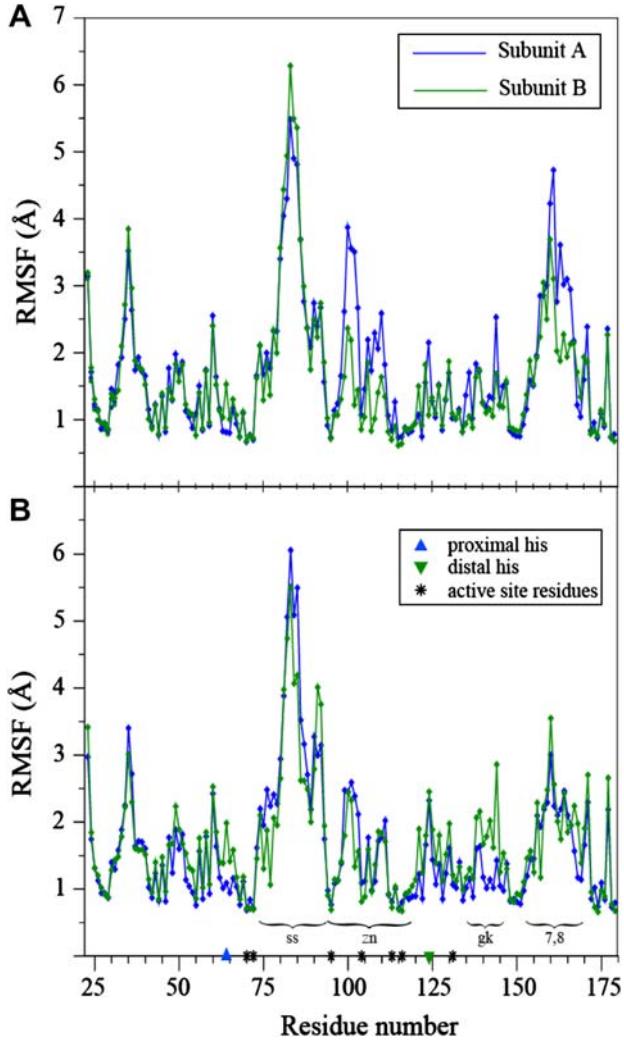

Figure 5. Per-residue RMSF of subunit A (blue) and subunit B (green) for HdSOD (A) and CO-HdSOD (B). ss = SS subloop; zn = Zn subloop; gk = Greek key loop; and 7,8 = 7,8 loop.

the structured β-barrel region. The first 5 ns of each simulation have been removed from all the following analyses that, therefore, have been carried out from 5 to 100 ns of simulation time.

The per-residue RMSF for the HdSOD and CO-HdSOD systems are shown in Figure 5 panels A and B, respectively. In HdSOD, the SS subloop (residues Glu73-Gly93) is the most fluctuating region in both subunits, while the Zn and 7,8 loops have larger fluctuations in subunit A than in B (Figure 5, panel A). An asymmetric dynamic of the two subunits has been often observed in other prokaryotic SODs, and has been attributed to an inter-domain communication that modulates the enzymatic catalytic cycle (Desideri & Falconi, 2003; Falconi et al., 2001). In line, the asymmetric dynamics of the HdSOD subunits involves regions (the Zn and 7,8 loops) belonging to the active site.

It is interesting to note that the asymmetric behavior of the two subunits nearly disappears upon binding of the CO molecule (Figure 5, panel B), with the exception of the Greek key loop that shows an increase of fluctuation in the subunit B as compared to subunit A likely due to the loss of the Fe–His124 interaction. The great reduction in the asymmetric subunit dynamics upon CO binding demonstrates a role of the heme group, bound at the subunit interface, in mediating long range communications.

Hydrogen bond analysis

The number of protein–protein hydrogen bonds made by the different enzyme regions and present for more than 80% of the simulation time are reported in Table 2. The large majority of the hydrogen bonds are formed in the structured region of the β-barrel. Subunit A has a smaller number of stable hydrogen bonds in HdSOD, while their number increases in CO-HdSOD, up to nearly the same value observed in subunit B, again showing that the

Table 2. Protein–protein hydrogen bonds in different enzyme regions.

	HdSOD		CO-HdSOD	
	Subunit A	Subunit B	Subunit A	Subunit B
β-Barrel	33	39	38	39
SS subloop	5	3	4	5
Zn subloop	4	5	6	7
Greek key loop	1	2	2	1
7,8 loop	1	1	4	3
Residues < 10 Å from Fe	4	6	7	6

asymmetry between the HdSOD subunits disappears upon binding of the CO molecule.

The greater difference in number of hydrogen bonds between HdSOD and CO-HdSOD is observed in the 7,8 loop, where the two hydrogen bonds observed in HdSOD (one in each subunit) increases to four and three in subunits A and B of CO-HdSOD, respectively. Four interactions, in particular, are observed only in the CO-HdSOD system; all involving histidine residues (His70-Asp155, His151-Gly168, Ser158-His104 in subunit A and Gly153-His67 in subunit B), with the first two copper coordinated. The increase in number of hydrogen bonds upon binding of CO is observed also in the Zn subloop, with two interactions never observed among the stable hydrogen bonds of HdSOD: i.e. Ser158-His104 in subunit A, already mentioned, and Tyr106-His157 in subunit B. Table 2 shows also an increased number of interactions involving residues in close proximity the Fe-heme ion in subunit A of CO-HdSOD. Two out of its seven stable interactions are not observed in HdSOD: i.e. Leu62-Gly126 and His64-Val122. Note that this last contact regards the proximal histidine, interacting also with the Fe-heme ion.

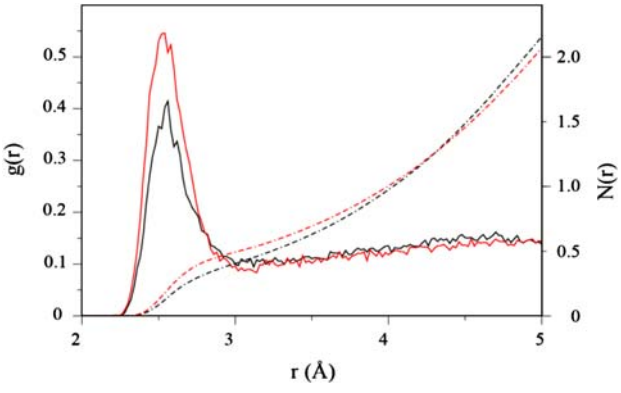

Figure 6. Radial distribution functions (full lines) and running integration numbers (dash dotted lines) for Cu and water oxygen atoms in HdSOD (black lines) and CO-HdSOD (red lines).

Since the protein–protein hydrogen bonds show great difference in the interaction network around the Cu,Zn site between HdSOD and CO-HdSOD, we have further investigated the structure of the Cu(II) ion in the two systems, searching for the number of interacting water molecules. Radial distribution functions and corresponding integration numbers for Cu and water oxygen atoms in HdSOD and CO-HdSOD (black and red line, respectively) are shown in Figure 6. The distribution of water molecules around the copper of the active site clearly shows that binding of the CO molecule to the heme has the effect to raise the water accessibility of the copper atom at short distance. At distance greater than 4 Å, the water distribution became nearly equal in the two systems.

Copper loss by CO-HdSOD

Previous studies have shown that bacterial Cu,ZnSODs have a lower affinity for the active site copper ion with respect to eukaryotic enzymes of the same class, as demonstrated by their tendency to lose activity when incubated in presence of chelating agents (Gabbianelli et al., 2004). It is noted that the rate of copper loss and catalytic efficiency may be increased by point mutations of residues located at the dimer interface (Stroppolo et al., 2000, 2001), while mutations at the subunit interface in human SOD have been related to neurological diseases such as familial amyotrophic lateral sclerosis (Hough et al., 2004). Therefore, small structural perturbations occurring quite far from the active site may significantly affect the accessibility of the copper ion or the stability of copper binding to the protein. To verify the hypothesis that CO binding to the heme group located at the dimer interface of HdSOD could have a long range effect on the catalytic copper ion, we have tested the stability of copper binding in a mutant form of the enzyme lacking the N-terminal metal-binding domain (Battistoni et al., 2001; D'Angelo et al., 2005). The residual superoxide dismutase activity of HdSOD and heme-devoid HdSOD after incubation with CO and BCS, a chelating agent able to tightly bind copper, was 27.9(±5.6)% and 42.3 (±4.7)%, respectively, indicating that CO binding to heme induces structural rearrangements that facilitate copper release from the active site. A Student's *t*-test confirmed the statistical significance of this difference ($p = 0.015$).

Conclusions

We have applied the "dynamic XANES" procedure to heme Fe(II) HdSOD and CO-HdSOD demonstrating that, as in the case of heme Fe(II) neuroglobin D'Angelo et al., 2010, the inclusion of the structural disorder effects modeled by MD simulations allows a quantitative reproduction of the XANES spectra. Furthermore,

we have shown that simulation of the systems, in which the heme Fe(II) equilibrium geometry is obtained by the EXAFS analysis, perfectly reproduces the experimental data, thus resolving the reported discrepancy between EXAFS and XANES data (D'Angelo et al., 2010).

Moreover, the accuracy of the "dynamic XANES" analysis corroborates the reliability of the force field used and the consistency of the structural dynamic information obtained from the MD simulations. RMSD analysis of the 100 ns long MD simulations highlighted a structural modification in the β-barrel structured region of the CO bound system, not observed in the deoxy system. We observed that binding of the CO molecule produces a strong reduction in the asymmetric fluctuations of the two subunits, as revealed by the per-residue RMSF. Also, the hydrogen bond analysis shows a long range effect of the heme group on the Cu active site structure, demonstrated by the greater number of stable hydrogen bonds in CO-HdSOD, involving also copper binding histidines. A long range communication between the intersubunit surface and the copper active site has been already observed in prokaryotic Cu,Zn SOD (Desideri & Falconi, 2003; Stroppolo et al., 2000). It has been shown that single mutations at the subunit interface of the SOD from *Photobacterium leiognathi* are able to enhance the enzyme catalytic efficiency and that this feature is paralleled by a proportional increase in copper accessibility, as revealed, for example, by a faster inactivation rate upon incubation with a chelating agent (Stroppolo et al., 1998, 2001). Here, we have provided evidence that in HdSOD the binding of the CO molecule to the porphyrin ring located at the subunit interface increases the rate of the copper chelation from an external compound when compared with the same experimental condition in the absence of the heme group; and it makes the copper ion more accessible to the water as evidenced by MD simulations. Although the conditions used to reduce iron and favor CO binding prevented the measurements of SOD catalytic activity by standard assays (data not shown), our findings indicate that the subtle rearrangements occurring at the subunit interface following the binding of a small gaseous ligand to the heme group may actually modulate copper accessibility in HdSOD and suggest that this may lead to an increase in copper reactivity.

In conclusion, we gained *in silico* and *in vitro* evidences concurring in proposing a role of HdSOD as a heme-based-sensor protein in which conformational changes, triggered by the heme group, could help *H. ducreyi* to adapt at fluctuating levels of gaseous molecules, such as carbon monoxide or nitric oxide. Based on this picture, in the presence of these gasses, the HdSOD would be able to increase its superoxide dismutation activity to subtract superoxide substrate and to prevent the formation of the dangerous peroxynitrite, the molecule generated by the reaction of nitric oxide with superoxide, which is even more harmful to the cell than superoxide. Further investigation to validate this attractive hypothesis is thus desirable.

Abbreviations

Hd	*Haemophilus ducreyi*
SOD	Cu,Zn superoxide dismutase
CO	carbon monoxide
MD	molecular dynamics
XAS	X-ray absorption spectroscopy
XANES	X-ray absorption near edge structure
EXAFS	extended X-ray absorption fine structure
ESRF	European Synchrotron Radiation Facility
HL	Hedin-Lundqvist
fwhm	full width at half-maximum
HEPES	(4-(2-hydroxyethyl)-1-piperazineethanesulfonic acid
BCS	bathocuproinedisulfonic acid
RMSD	root mean square deviations
RMSF	root mean square fluctuations

Acknowledgments

We thank Simonetta Antonaroli for her help in carrying out experiments with NO and Alessandro Grottesi and Andrea Coletta for helpful discussions. This work was supported by CASPUR with the Standard HPC Grant 2010 entitled "A combined X-ray absorption spectroscopy, Molecular Dynamics simulations and Quantum Mechanics calculation procedure for the structural characterization of ill-defined systems" and with a doctorate fellowship to SDS.

References

Battistoni, A., Pacello, F., Mazzetti, A.P., Capo, C., Kroll, S.J., Langford, P., … Rotilio, G. (2001). A histidine-rich metal binding domain at the N terminus of Cu,Zn-superoxide dismutases from pathogenic bacteria: A novel strategy for metal chaperoning. *The Journal of Biological Chemistry, 276*, 30315–30325.

Becke, A.D. (1993). Density-functional thermochemistry. III. The role of exact exchange. *Journal of Chemical Physics, 98*, 5648–5652.

Benfatto, M., & Della Longa, S. (2001). Geometrical fitting of experimental XANES spectra by a full multiple scattering procedure. *Synchrotron Radiation, 8*, 1087–1094.

Berendsen, H.J.C., Postma, J.P.M., van Gunsteren, W.F., & Hermans, J. (1981). Interaction models for water in relation to protein hydration. In B. Pullman (Ed.), *Intermolecular forces* (pp. 331–342). Dordrecht: D. Reidel.

Berendsen, H.J.C., van der Spoel, D., & van Drunen, R. (1995). GROMACS: A message-passing parallel molecular dynamics implementation. *Computer Physics Communications, 91*, 43–56.

Breneman, C.M., & Wiberg, K.B. (1990). Determining atom-centered monopoles from molecular electrostatic potentials – the need for high sampling density in formamide conformational-analysis. *Journal of Computational Chemistry, 11*, 361–373.

Bussi, G., Donadio, D., & Parrinello, M. (2007). Canonical sampling through velocity rescaling. *Journal of Chemical Physics, 126*, 14101–14108.

D'Angelo, P., Della Longa, S., Arcovito, A., Anselmi, M., Di Nola, A., & Chillemi, G. (2010). Dynamic investigation of protein metal active site: The interplay of XANES and molecular dynamics simulations. *Journal of the American Chemical Society, 132*, 14901–14909.

D'Angelo, P., Lapi, A., Migliorati, V., Arcovito, A., Benfatto, M., Roscioni, O.M., … Della Longa, S. (2008). X-ray absorption spectroscopy of hemes and hemeproteins in solution: Multiple scattering analysis. *Inorganic Chemistry, 47*, 9905–9918.

D'Angelo, P., Pacello, F., Mancini, G., Proux, O., Hazemann, J.L., Desideri, A., & Battistoni, A. (2005). X-ray absorption investigation of a unique protein domain able to bind both Cu(I) and Cu(II) at adjacent sites of the N-terminus of Haemophilus ducrey X-ray absorption investigation of a unique protein domain able to bind both Cu(I) and Cu(II). *Biochemistry, 44*, 13144–13150.

D'Angelo, P., Zitolo, A., Pacello, F., Mancini, G., Proux, O., Hazemann, J.L., … Battistoni, A. (2010). Fe-heme structure in Cu,Zn superoxide dismutase from Haemophilus ducreyi by X-ray absorption spectroscopy. *Archives of Biochemistry and Biophysics, 498*, 43–49.

De Maria, F., Pedersen, J.Z., Caccuri, A.M., Antonini, G., Turella, P., Stella, L., Lo Bello, M., Federici Falconi, M., Parrilli, L., Battistoni, A., & Desideri, A. (2002). Flexibility in monomeric Cu,Zn superoxide dismutase detected by limited proteolysis and molecular dynamics simulation. *Proteins, 47*, 513–520.

Desideri, A., & Falconi, M. (2003). Cu,Zn superoxide dismutases. *Biochemical Society Transactions, 31*, 1322–1325.

Essmann, U., Perera, L., Berkowitz, M.L., Darden, T., Lee, H., & Pedersen, L.G.A. (1995). A smooth particle mesh ewald method. *Journal of Chemical Physics, 103*, 8577–8593.

Falconi, M., Stroppolo, M.E., Cioni, P., Sergi, A., Ferrario, M., & Desideri, A. (2001). Cu,Zn superoxide dismutase: A spectroscopic and molecular dynamics simulation study. *Biophysical Journal, 80*, 2556–2567.

Frisch, M.J., Trucks, G.W., Schlegel, H.B., Scuseria, G.E., Robb, M.A., Cheeseman, J.R., … Fox, D.J. (2009). *Gaussian 09, Revision D02*. Wallingford, CT: Gaussian.

Gabbianelli, R., D'Orazio, M., Pacello, F., O'Neil, P., Nicolini, L., Rotilio, G., & Battistoni, A. (2004). Distinctive functional features in prokaryotic and eukaryotic Cu,Zn superoxide dismutases. *The Journal of Biological Chemistry, 385*, 749–754.

Gilles-Gonzalez, M.A., & Gonzalez, G. (2005). Heme-based sensors: Defining characteristics, recent developments, and regulatory hypotheses. *Journal of Inorganic Biochemistry, 99*, 1–22.

Harvey, J.N. (2000). DFT computation of the intrinsic barrier to CO geminate recombination with heme compounds. *Journal of the American Chemical Society, 122*, 12401–12402.

Hess, B., Kutzner, C., van der Spoel, D., & Lindahl, E. (2008). Algorithms for highly efficient, load-balanced, and scalable molecular simulation. *Journal of Chemical Theory and Computation, 4*, 435–447.

Hough, M.A., Grossmann, J.G., Antonyuk, S.V., Strange, R.W., Doucette, P.A., Roderiguez, J., … Hasnain, S.S. (2004). Dimer destabilization in superoxide dismutase may result in disease-causing properties: Structures of motor neuron disease mutants. *Proceedings of the National Academy of Sciences, 101*, 5976–5981.

Li, J., Ai, Y.J., Xie, Z.Z., & Fang, W.H. (2008). How CO binds to hexacoordinated heme in neuroglobin protein. *The Journal of Physical Chemistry B, 112*, 8715–8723.

Loew, G.H., & Harris, D.L. (2000). Role of the Heme Active Site and Protein Environment in Structure, Spectra, and Function of the Cytochrome P450s. *Chemical Reviews, 100*, 407–420.

Marklund, S., & Marklund, G. (1974). Involvement of the superoxide anion radical in the autoxidation of pyrogallol. A convenient assay for superoxide dismutase. *Journal of Biochemistry, 47*, 469–474.

McMahon, B.H., Stojkovic, B.P., Hay, P.J., Martin, R.L., & Garcia, A.E. (2000). Microscopic model of carbon monoxide binding to myoglobin. *The Journal of Chemical Physics, 113*, 6831–6850.

Muller, J.B., Jepsen, O., & Wilkins, J.W. (1982). X-ray absorption spectra: K-edges of 3d transition metals, L-edges of 3d and 4d metals, and M-edges of palladium. *Solid State Communications, 42*, 365–368.

Negari, S., Sulpher, J., Pacello, F., Ingrey, K., Battistoni, A., & Lee, B.C. (2008). A role for *Haemophilus ducreyi* Cu,Zn SOD in resistance to heme toxicity. *BioMetals, 21*, 249–258.

Oostenbrink, C., Villa, A., Mark, A.E., & van Gunsteren, W.F. (2004). A biomolecular force field based on the free enthalpy of hydration and solvation: The GROMOS force-field parameter sets 53A5 and 53A6. *Journal of Computational Chemistry, 25*, 1656–1676.

Pacello, F., Langford, P.R., Kroll, J.S., Indiani, C., Smulevich, G., Desideri, A., … Battistoni, A. (2001). A novel heme protein, the Cu,Zn-superoxide dismutase from *Haemophilus ducreyi*. *Journal of Biological Chemistry, 276*, 30326–30334.

Schaefer, A., Horn, H., & Ahlrichs, R. (1992). Fully optimized contracted Gaussian basis sets for atoms Li to Kr. *The Journal of Chemical Physics, 97*, 2571–2577.

Shen, J., Wong, C.F., Subramaniam, S., Albright, T.A., & McCammon, J.A. (1990). Partial electrostatic charges for the active center of Cu,Zn superoxide dismutase. *Journal of Computational Chemistry, 11*, 346–350.

Smith, D.M.A., Dupuis, M., & Straatsma, T.P. (2005). Multiplet splittings and other properties from density functional theory: An assessment in iron-porphyrin systems. *Molecular Physics, 103*, 273–278.

Stroppolo, M.E., Pesce, A., D'Orazio, M., O'Neill, P., Bordo, D., Rosano, C., … Desideri, A. (2001). Single mutations at the subunit interface modulate copper reactivity in photobacterium leiognathi Cu,Zn superoxide dismutase. *Journal of Molecular Biology, 308*, 555–563.

Stroppolo, M.E., Pesce, A., Falconi, M., O'Neill, P., Bolognesi, M., & Desideri, A. (2000). Single mutation at the intersubunit interface confers extra efficiency to Cu,Zn superoxide dismutase. *FEBS Letters, 483*, 17–20.

Stroppolo, M.E., Sette, M., O'Neill, P., Polizio, F., Cambria, M.T., & Desideri, A. (1998). Cu,Zn superoxide dismutase from photobacterium leiognathi is an hyperefficient enzyme. *Biochemistry, 37*, 12287–12292.

Törő, I., Petrutz, C., Pacello, F., D'Orazio, M., Battistoni, A., & Djinović-Carugo, K. (2009). Structural basis of heme binding in the Cu,Zn superoxide dismutase from *Haemophilus ducreyi*. *Journal of Molecular Biology, 386*, 406–418.

Vallone, B., Nienhaus, K., Matthes, A., Brunori, M., & Nienhaus, G.U. (2004). The structure of murine neuroglobin: Novel pathways for ligand migration and binding. *Proceedings of the National Academy of Sciences USA, 101*, 17351–17356.

Van Gunsteren, W.F., Billeter, S., Eising, A., Hunenberger, P., Kruger, P., Mark, A.E., …, & Tironi, I. (1996). *The GROMOS96 manual and user guide*. Zurich: BIOMOS BV.

Vos, M.H., Battistoni, A., Lechauve, C., Marden, M.C., Kiger, L., Desbois, A., … Liebl, U. (2008). Ultrafast heme-residue bond formation in six-coordinate heme proteins: Implications for functional ligand exchange. *Biochemistry, 47*, 5718–5723.